Rarefaction effects on shear driven oscillatory gas flows: A direct simulation Monte Carlo study in the entire Knudsen regime

Jae Hyun Park
Beckman Institute for Advanced Science and Technology, University of Illinois at Urbana-Champaign, Urbana, Illinois 61801

P. Bahukudumbi and Ali Beskok[a)]
Department of Mechanical Engineering, Texas A&M University, College Station, Texas 77843

(Received 21 July 2003; accepted 21 October 2003; published online 24 December 2003)

A complete mathematical description of oscillatory Couette flows within the framework of kinetic theory is not available in the literature. Motivated by this and their vast engineering applications, we present a parametric study of time-periodic oscillatory Couette flows using the unsteady direct simulation Monte Carlo (DSMC) method. Computations are performed as a function of the Knudsen (Kn) and Stokes (β) numbers, in the entire Knudsen regime ($\mathrm{Kn} \leqslant 100$) and a wide range of Stokes numbers ($\beta \leqslant 7.5$). The DSMC results are validated using a recently developed semianalytical/empirical model that is applicable for quasisteady flows ($\beta \leqslant 0.25$) in the entire Knudsen regime, and for any Stokes number flow in the slip flow regime ($\mathrm{Kn} \leqslant 0.1$). In addition, we derived an analytical solution of the linearized collisionless Boltzmann equation for oscillatory Couette flows, and utilized this to validate the DSMC results in the free-molecular flow regime. Dynamic response of the flow, including the velocity profiles, phase angle, wave speed, shear stress, and the penetration depth for high Stokes number flows are presented. Increasing the Stokes number at fixed Kn, we observed formation of ''bounded Stokes layers,'' as expected. However, increasing the Knudsen number at fixed β results in ''bounded rarefaction layers,'' where the penetration depth continuously decreases with increasing the Kn. Interplay between the rarefaction and unsteadiness contributes to this interesting flow physics, and also introduces a new characteristic length scale to the problem.
 [DOI: 10.1063/1.1634563]

I. INTRODUCTION

Oscillatory Couette flow is the simplest approximation for time-periodic shear driven gas flows encountered in various microelectromechanical systems (MEMS), such as microaccelerometers, inertial sensors, and resonant filters.[1–4] Although this classical problem has been investigated extensively using continuum-based flow models,[2] a fundamental problem arises with miniaturization of device components and packaging MEMS at subatmospheric pressures.[1] Analysis of such conditions requires consideration of rarefaction effects, which are characterized by the Knudsen number, defined as $\mathrm{Kn}=\lambda/L$, where λ is the gas mean-free-path and L is a characteristic flow length scale. Based on the Knudsen number, gas flows can be *qualitatively* classified as continuum ($\mathrm{Kn}<0.01$), slip ($0.01<\mathrm{Kn}<0.1$), transition ($0.1<\mathrm{Kn}<10$), and free-molecular ($\mathrm{Kn}>10$) flow.[5] Most existing MEMS devices operate in the slip and early transition regimes. Further miniaturization of device components will push this limit to the transition and free-molecular flow regimes. Hence, successful design of these microfluidic systems is faced with the challenge of better understanding of micron and submicron scale physics and transport processes in a wide range of flow regimes.

While substantial literature on steady rarefied Couette flows exists, a thorough kinetic theory treatment of time-periodic Couette flows is not available. Although microscopic simulation methods such as the Boltzmann solvers or the DSMC can be used to investigate the flow physics, such methods are very difficult to apply to engineering problems that involve unsteady flows due to the computational complexity and storage requirements. The difficulty in numerical solution of the Boltzmann equation arises due to the nonlinearity, complexity of the collision integral terms, and the multidimensionality of the equation. DSMC is a particle-based method for gas flows, and it is applicable to all flow regimes.[6] The DSMC uses a stochastic algorithm to evaluate collision probabilities and scattering distributions. In recent work by Wagner,[7] it has been rigorously proved that the DSMC is equivalent to a Monte Carlo solution of an equation that is similar to the Boltzmann equation. Although simpler theoretical models such as the Navier–Stokes equation with slip correction and the collisionless Boltzmann equation can be used in the slip and free-molecular flow regimes, respectively, there is a lack of theoretical understanding and reliable models in the transition flow regime. Numerically, the DSMC method of Bird[6] remains the simulation tool of choice to obtain solutions for gas flows in the transition flow regime. From the time of its introduction, the DSMC method has been widely used for simulation of rarefied gas flows. More recently, the DSMC method has been increasingly used

[a)]Author to whom correspondence should be addressed. Telephone: (979) 862-1073; fax: (979) 862-2418; electronic mail: abeskok@mengr.tamu.edu

to simulate flows in micro- and nanoscale devices. Since most MEMS devices contain moving components, unsteady DSMC computations are necessary to study fluid–structure interaction in such systems. Despite their practical importance, analyses of unsteady rarefied gas flows are not common in the literature.

In the following, we review some of the previous investigations that utilize the DSMC method or the Boltzmann equation to analyze time-periodic/unsteady rarefied flows. Stefanov *et al.*[8] used the unsteady DSMC method to investigate time-periodic oscillatory flows in the near-continuum/slip flow regime (Kn$=0.01$). The unsteady motion was induced by a combination of longitudinal and transverse time-periodic oscillations of a surface. These simulations were performed in the limit where the compressibility and viscous heating are important. Hadjiconstantinou and Garcia[9] and Hadjiconstantinou[10] analyzed sound wave propagation in micro/nanoscale flows using unsteady DSMC, and verified their results by comparisons with the continuum and linearized Boltzmann solutions. Sharipov *et al.*[11] studied sound propagation in the free-molecular regime using the linearized collisionless Boltzmann equation. Park and Baek[12] and Park *et al.*[13] applied unsteady DSMC to investigate heat transfer in oscillatory rarefied gas flows. In most of these previous investigations, normal oscillations to the surface are considered. In previous work, we developed a generalized slip-based empirical model for oscillatory Couette flows that can accurately predict the velocity profiles and shear stress for Kn$\leqslant 12$ in the quasisteady flow limit.[14] This new model was validated using unsteady DSMC results. This previous work excluded the high Stokes number rarefied flows, where the nonequilibrium effects become dominant, especially when the plate oscillation frequency is comparable to the molecular collision frequency. This work is an extension of our previous research, and it is motivated by the lack of oscillatory Couette flow studies in the pertinent literature.

This paper is organized as follows: In Sec. II, we briefly review the DSMC method used in this study with specific emphasis on the choice of simulation parameters. The continuum-based slip solution for quasisteady flows developed in an earlier work[14] is summarized in Sec. III. In Sec. IV, we derive the free-molecular solution for oscillatory Couette flows using the collisionless Boltzmann equation. In Sec. V, DSMC results are compared with the slip-model solution and the theoretical solution based on the collisionless Boltzmann equation. Dynamic response characteristics of the medium are presented for a wide range of Stokes numbers in the entire Knudsen regime. Also, the influence of Kn and β on wall shear stress, and penetration depth are examined. Finally, we present the conclusions of our study.

II. PROBLEM DEFINITION AND UNSTEADY DSMC METHOD

We consider rarefied gas flow between two infinite parallel plates that are a distance L apart, where the top plate oscillates harmonically in the lateral direction and the bottom plate is stationary, as shown in Fig. 1. Two plates are maintained at the same temperature $T_w=273$ K. The gas medium

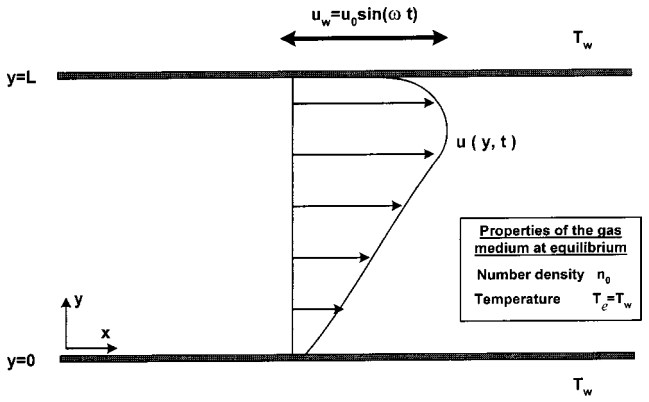

FIG. 1. Schematic of oscillatory Couette flow.

is initially at rest, and it has an equilibrium number density n_0, and equilibrium temperature T_e that is equal to the wall temperature T_w.

Oscillatory rarefied Couette flows are characterized by the Knudsen (Kn) and Stokes (β) numbers. The Stokes number represents balance between the unsteady and viscous effects. It can also be interpreted as the ratio of the diffusion and oscillation characteristic time scales, and it is defined as[1,2]

$$\beta=\sqrt{\frac{\omega L^2}{\nu}}=\left(\frac{L^2/\nu}{1/\omega}\right)^{1/2}, \tag{1}$$

where ν is the kinematic viscosity and ω is the oscillation frequency. Here, we must note that Stokes number in this context is *identical* to the Womersley number used in pulsating flows.[15,16] However, we chose to use the Stokes number instead, since our work is on oscillatory shear-driven viscous flows, and on Stokes' second problem.[17]

We performed a series of DSMC simulations of oscillatory Couette flows for various combinations of Kn and β. The DSMC code used in this study was based on the unsteady algorithm presented by Bird.[6] The code has been successfully applied to the analysis of microscale heat transfer in oscillating rarefied gas flows in previous work.[12,13] In the simulations, we utilized the hard sphere (HS) model for molecular collision, and the no-time-counter (NTC) scheme is adapted for collision pair selection.[6] The choice of the HS model facilitates easy comparisons with the theoretical solutions of the linearized Boltzmann equation[10] and also enables easier code implementation. We simulated argon gas (molecular mass $m=6.63\times10^{-26}$ kg, hard sphere diameter $d_{\mathrm{HS}}=3.66\times10^{-10}$ m) with a reference temperature $T_e=273$ K. The walls are assumed to be fully accommodating. Hence, the particles are reflected from the walls according to a Maxwellian distribution with wall velocity and temperature. Simulation parameters are chosen so that the compressibility and viscous heating effects are negligible. Although the gas temperature increases with increased oscillation frequency, the maximum temperature rise in the simulations was less than 2%.

We have utilized more than 100 simulated particles per cell. The entire domain was discretized into 40–100 equally

spaced cells, to ensure that the cell size (Δx) is smaller than the mean free path for all simulations. Finer grid is used for high Stokes number flows to resolve the flow inside the Stokes layers, while a coarser grid is used for low Stokes number flows. In the choice of the simulation time step (Δt), we had to consider four different limitations. First, Δt has to be significantly smaller than the mean collision time to ensure accurate simulations. Second, the cell size should be smaller than the mean free path, and the molecules should not move across more than one cell between two consecutive time steps. Hence, $\Delta t \ll \Delta x/c_0$, where $c_0=\sqrt{2RT_e}$ is the most probable velocity. Third, the time period of oscillations can become smaller than the mean collision time; hence, $\Delta t \ll 2\pi/\omega$. Fourth, choice of L and ν in a microscale DSMC simulation can result in a relatively small viscous diffusion time, which scales as L^2/ν; hence, $\Delta t \ll L^2/\nu$. In all simulations, the time step has been chosen to satisfy all four constraints. The range of the total simulation time was around 3 to 18 time periods ($T_0=2\pi/\omega$). This ensures that the transients starting from the quiescent initial conditions decay, and time-periodic state is achieved. In unsteady DSMC, ensemble average at each time step replaces the time average used in steady computations. In this study, ensemble averaging is performed over 5000 different realizations of the stochastic process for each time step.

In all simulations, amplitude of the oscillating wall is kept constant at $u_0=100$ m/s, maintaining relatively low Mach number flows so that the compressibility effects are negligible. The gas number density (n_0), excitation frequency (ω), and the characteristic system length (L) are adjusted to simulate different combinations of Kn and β. Although the *dimensional parameters* utilized in the simulations lead to unique values of the Knudsen and Stokes numbers, we wanted to ensure that there are no other unaccounted nondimensional parameters involved in the problem. For example, ratio of the mean molecular collision time (t_c) to the time scale of oscillations (ω^{-1}) can be an indication of nonequilibrium effects. However, it can be shown that $\omega t_c=5/16\sqrt{2\pi/\gamma}(\beta\,\mathrm{Kn})^2$ for hard sphere gases like argon. This result indicates that for a given Kn and β, the nondimensionalized DSMC results should be *dynamically similar*, regardless of the dimensional parameters used in the simulations. To validate the dynamic similarity, we performed several simulations with various combinations of ω and t_c. All these simulation results were indistinguishable from each other, with the exception of statistical fluctuations induced by the DSMC. Statistical scatter of DSMC computations will be addressed in the Results and Discussions section.

III. CONTINUUM-BASED SLIP MODELS

The Navier–Stokes equation, along with the appropriate slip boundary conditions, can be used to investigate oscillatory Couette flows in the slip-flow regime. In previous work,[14] using DSMC, we have shown that the continuum-based first-order slip models are invalid beyond Kn=0.1 for steady and quasisteady flows ($\beta \leqslant 0.25$). In addition, we have developed an extended slip-flow model that can accurately predict the velocity distribution and shear stress for steady and quasisteady flows in a wide Knudsen number range (Kn$\leqslant$12). The new model was based on the Navier–Stokes equation with a modified velocity slip boundary condition. In the following we summarize this *empirical* model.

A. Velocity model

For a small amplitude lateral motion that does not generate any streamwise pressure gradients, the momentum equation reduces to the following:

$$\frac{\partial u(y,t)}{\partial t}=\nu\frac{\partial^2 u(y,t)}{\partial y^2}. \tag{2}$$

For a sinusoidal velocity excitation, a velocity response of $u(y,t)=\Im\{V(y)\exp(j\omega t)\}$ is expected, where the symbol $\Im$ denotes the imaginary part of a complex expression, $V(y)$ is the velocity amplitude at location y, and $j=\sqrt{-1}$. Neglecting thermal creep effects, the modified velocity slip boundary condition becomes

$$u-u_w=\frac{2-\sigma_v}{\sigma_v}\alpha_m\lambda\frac{\partial u}{\partial y}, \tag{3}$$

where u is the gas slip velocity, u_w is the wall velocity, and α_m is the modified slip coefficient given by

$$\alpha_m=1.298+0.718\tan^{-1}(-1.175\ \ \mathrm{Kn}^{0.586}). \tag{4}$$

This slip boundary condition converges to a first-order slip condition in the slip flow regime, and it is indeed a high-order slip model for Kn$\geqslant$0.1. This can be shown via a Taylor series expansion of α_m in Kn.[14] Using Eq. (2) and the slip boundary condition given by Eq. (3), we obtain the following time-dependent velocity distribution:

$$u(y,t)=\Im\left[\left(u_0\frac{\sinh(\sqrt{j}\beta Y)+\sqrt{j}\beta\alpha_m\mathrm{Kn}\cosh(\sqrt{j}\beta Y)}{(1+j\beta^2\alpha_m^2\,\mathrm{Kn}^2)\sinh(\sqrt{j}\beta)+2\sqrt{j}\beta\alpha_m\mathrm{Kn}\cosh(\sqrt{j}\beta)}\right)\exp(j\omega t)\right], \tag{5}$$

where $Y=y/L$. This is a *general* solution for the velocity profile that captures the no-slip solution simply by setting Kn=0, and the first-order slip solution by setting $\alpha_m=1.111$. In Ref. 14, we have shown that the above equation is valid for *any* Stokes number in the continuum and slip flow regimes (Kn$\leqslant$0.1), and it is also valid for quasisteady flows ($\beta\leqslant 0.25$) for Kn $\leqslant$12.

B. Shear stress model

In Ref. 14, we derived an empirical shear stress model that is uniformly valid in the entire Knudsen regime for steady, and quasisteady oscillatory Couette flows. The model was based on an effective viscosity given below:

$$\mu_{\text{eff}}=\frac{\mu_0}{2}\frac{a\,\text{Kn}+2b}{a\,\text{Kn}^2+c\,\text{Kn}+b}(1+2\alpha_m\,\text{Kn}),$$
$$a=0.530,\quad b=0.603,\quad c=1.628, \tag{6}$$

where μ_0 is the dynamic viscosity. Using the effective viscosity, the shear stress at the oscillating plate is given by

$$(\tau_{xy})_{qs}=\mu_{\text{eff}}\left.\frac{du(y,t)}{dy}\right|_{y=L}=\frac{\mu_0 u_0}{2L}\frac{a\,\text{Kn}+2b}{a\,\text{Kn}^2+c\,\text{Kn}+b}(1+2\alpha_m\,\text{Kn})$$
$$\times\Im\left[\left(\sqrt{j}\beta\,\frac{\cosh(\sqrt{j}\beta)+\sqrt{j}\beta\alpha_m\,\text{Kn}\sinh(\sqrt{j}\beta)}{(1+j\beta^2\alpha_m^2\,\text{Kn}^2)\sinh(\sqrt{j}\beta)+2\sqrt{j}\beta\alpha_m\,\text{Kn}\cosh(\sqrt{j}\beta)}\right)\exp(j\omega t)\right]. \tag{7}$$

In the limit of $\beta\to 0$, the model reduces to shear stress for steady Couette flows. In Sec. V, we present comparisons between the model predictions and the shear stress obtained from the DSMC simulations at various Kn and β conditions.

IV. FREE-MOLECULAR SOLUTION

In this section, we derive the velocity distribution and shear stress for oscillatory Couette flows in the free-molecular flow limit ($\text{Kn}\geqslant 10$). Our objectives are to provide a theoretical solution to compare and validate our DSMC results, and enhance our understanding of flow physics in this regime. As the Knudsen number is increased, intermolecular collisions become negligible compared to the molecule/surface collisions. Therefore, the flow can be modeled using the collisionless Boltzmann equation given as

$$\frac{\partial f}{\partial t}+\eta\frac{\partial f}{\partial y}=0, \tag{8}$$

where f is the velocity distribution function and η is the cross-flow (y) component of the molecular velocity. Due to the simple geometry f changes only in the cross-flow direction, and there are no external force fields. We assume that both top and bottom walls are fully diffusive, and a sinusoidal excitation is exerted on the top wall ($y=L$). The boundary conditions for Eq. (8) are

$$f(y=0)=f_0=\frac{\kappa^3}{\pi^{3/2}}\exp[-\kappa^2(\xi^2+\eta^2+\zeta^2)];\quad \eta>0, \tag{9}$$

$$f(y=L;u_w)=\frac{\kappa^3}{\pi^{3/2}}\exp[-\kappa^2(\xi^2+(\eta-u_w)^2+\zeta^2)];\quad \eta<0, \tag{10}$$

where $u_w=u_0\sin(\omega t)$ and $\kappa=\sqrt{m/2k_BT_e}$. Here, T_e is the initial equilibrium temperature, k_B is the Boltzmann constant, and ξ and ζ are the streamwise and spanwise components of the molecular velocity, respectively. Diffuse reflections of gas molecules from the surfaces require that the reflected molecules have a Maxwellian distribution f_0, characterized by the velocity and temperature of the plates. Here, we assume that the amplitude of velocity oscillations is less than the speed of sound (a condition that is approximately satisfied by our DSMC results). This enables linearization of the collisionless Boltzmann equation and the boundary conditions. Following the work of Sone, the velocity distribution function can be decomposed into its equilibrium and fluctuating components as follows:[18,19]

$$f=f_0(1+\phi), \tag{11}$$

where ϕ is the normalized fluctuation. We can obtain the linearized forms of the Boltzmann equation and the boundary conditions by substituting Eq. (11) into Eqs. (8), (9), and (10) and neglecting all the higher-order terms in ϕ

$$\frac{\partial\phi}{\partial t}+\eta\frac{\partial\phi}{\partial y}=0, \tag{12}$$

$$\phi_0=\phi(y=0)=0;\quad \eta>0, \tag{13}$$

$$\phi_L=\phi(y=L)=2\kappa^2\xi u_w;\quad \eta<0. \tag{14}$$

In this study, we are interested in the streamwise component of the velocity u and the shear stress τ, which are defined as follows:

$$u=\int \xi\phi f_0\,d\xi\,d\eta\,d\varsigma, \tag{15}$$

$$\tau=\rho_0\int \xi\eta\phi f_0\,d\xi\,d\eta\,d\varsigma, \tag{16}$$

where $\int(\cdots)d\xi\,d\eta\,d\zeta$ shows integration over the velocity space, and ρ_0 is the mean density given by $\rho_0=n_0m$, with n_0 being the equilibrium number density, and m being the molecular mass. We apply Laplace transformation to Eq. (12) and the boundary conditions Eqs. (13) and (14) in order to calculate the integral formulations of the velocity and shear stress given by Eqs. (15) and (16). The Laplace transformed variables $\hat{\phi}$, $\hat{u}$, and $\hat{\tau}$ are given as

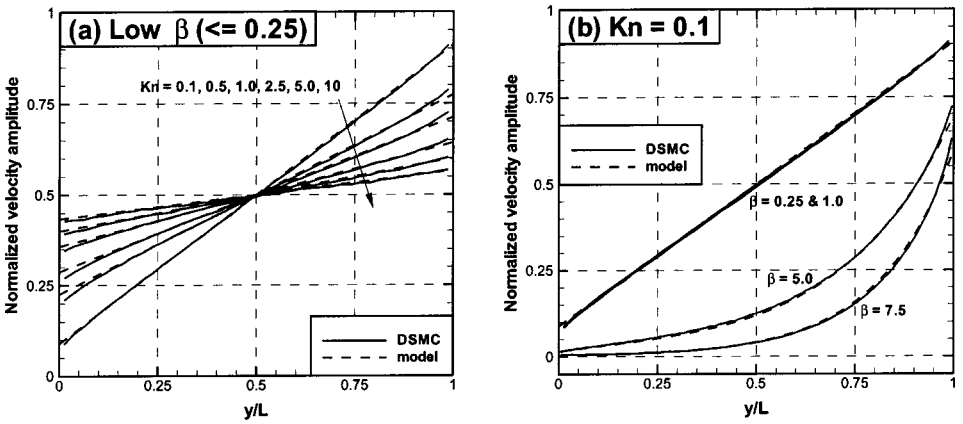

FIG. 2. Velocity amplitudes for quasi-steady and low Kn cases.

$$\hat{\phi}=\hat{\phi}_L \exp\left[-\frac{s}{\eta}(y-L)\right]=2\kappa^2\xi\hat{u}_w \exp\left[-\frac{s}{\eta}(y-L)\right];\quad \eta<0, \tag{17}$$

$$\hat{u}=\int \xi\hat{\phi}f_0\, d\xi\, d\eta\, d\zeta, \tag{18}$$

$$\hat{\tau}=\rho_0\int \xi\eta\hat{\phi}f_0\, d\xi\, d\eta\, d\zeta, \tag{19}$$

where s is the Laplace transformation variable. After eliminating $\hat{\phi}$ from Eqs. (17), (18), and (19), we obtain integral formulations for $\hat{u}$ and $\hat{\tau}$ as follows:

$$\hat{u}=\frac{\kappa}{\sqrt{\pi}}\int_0^\infty \hat{u}_w \exp\left(-\frac{s}{\eta''}(L-y)-\kappa^2\eta''^2\right)d\eta'', \tag{20}$$

$$\hat{\tau}=\rho_0\frac{\kappa}{\sqrt{\pi}}\int_0^\infty \hat{u}_w\eta'' \exp\left(-\frac{s}{\eta''}(L-y)-\kappa^2\eta''^2\right)d\eta'', \tag{21}$$

where $\hat{u}_w$ is the transformed function of u_w. Finally, the inverse Laplace transform provides u and τ as a function of y and t

$$u(y,t)=\frac{u_0}{\sqrt{\pi}}\int_{\kappa(L-y)/t}^\infty \sin\left[t-\frac{\kappa(L-y)}{\eta'}\right]\exp(-\eta'^2)d\eta', \tag{22}$$

$$\tau(y,t)=\frac{\rho_0 u_0}{\sqrt{\pi}}\int_{\kappa(L-y)/t}^\infty \eta' \sin\left[t-\frac{\kappa(L-y)}{\eta'}\right]\times\exp(-\eta'^2)d\eta'. \tag{23}$$

The gas velocity $\tilde{u}_{w,g}(t)$ and shear stress on the oscillating (top) wall are calculated as

$$\tilde{u}_{w,g}(t)=u(L,t)=\frac{u_0}{\sqrt{\pi}}\int_0^\infty \sin(\omega t)\exp(-\kappa^2\eta''^2)d\eta''=\frac{u_0}{2}\sin(\omega t)=u_{w,g}\sin(\omega t), \tag{24}$$

$$\tilde{\tau}_w=\tau(L,t)=\frac{\rho_0 u_0}{\sqrt{\pi}}\int_0^\infty \eta''\sin(\omega t)\exp(-\kappa^2\eta''^2)d\eta''=\frac{1}{2\sqrt{\pi}}\frac{\rho_0 u_0}{\kappa}\sin(\omega t)=\tau_w\sin(\omega t). \tag{25}$$

The magnitude of gas velocity on the oscillating plate and the corresponding shear stress are $u_w=u_0/2$ and $\tau_w=\frac{1}{2}\rho_0 u_0\sqrt{2k_BT_w/\pi}$, respectively. This shows that on the oscillating surface, the *magnitude of the gas velocity and shear stress for oscillatory Couette flows reaches the same asymptotic limit as their steady counterpart, when* $\mathrm{Kn}\to\infty$. This finding is also confirmed by the DSMC studies presented in the following section.

V. RESULTS AND DISCUSSIONS

In this section, we present our DSMC results in the slip, transition, and free-molecular flow regimes. The DSMC results are validated using predictions of the corresponding analytical models in the slip and free-molecular flow regimes. Effects and onset of statistical scatter in the simulations are discussed. Shear stress and penetration depth variations as a function of the Stokes and Knudsen numbers are presented.

A. Slip-flow regime and quasisteady flows

Figure 2 shows variation of the normalized velocity amplitude between the two surfaces. We compare the DSMC results with the predictions of the extended slip model[14] for (a) quasisteady flows in the entire Knudsen regime, and (b) slip flows for a wide range of Stokes numbers ($\beta\leqslant 7.5$). The velocity amplitudes are obtained by measuring the magnitude of the maximum velocity at different cross-flow (y) locations. Note that the generalized velocity model given by Eq. (5) converges to the first-order slip model for $\mathrm{Kn}<0.1$. Hence, only the predictions of the extended slip model are shown in the figure. For quasisteady flows, the velocity amplitude distribution always passes through $(y/L,u/u_0)=(0.5,0.5)$, and results in a linear velocity distribution with equal amount of slip on the oscillating and stationary walls. The extended slip model accurately matches the DSMC ve-

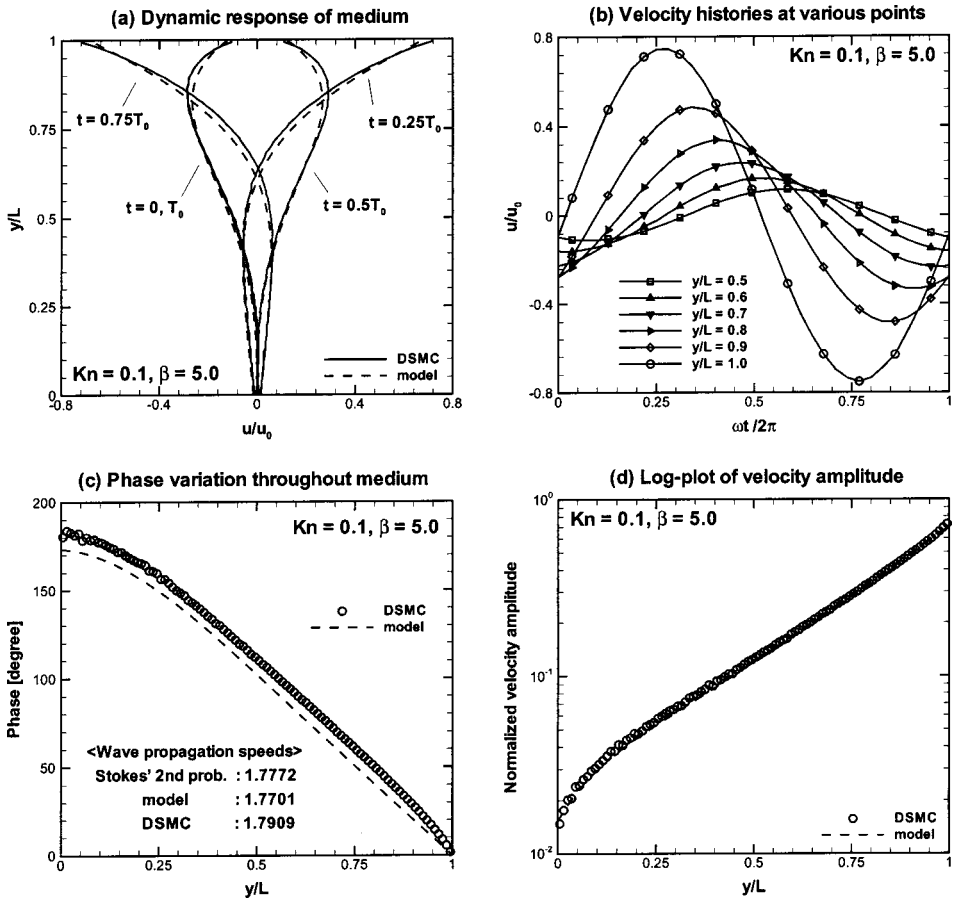

FIG. 3. Dynamic details for Kn=0.1 and $\beta=5.0$ flow.

locity profile for a wide range of Knudsen numbers ($\mathrm{Kn} \leqslant 12$). However, it fails to predict the Knudsen layers that are captured by the DSMC results, as expected from any continuum based model. The extended slip model is also valid for high Stokes number flows in the continuum and slip-flow regimes due to the use of the Navier–Stokes equations in its derivation. Figure 2(b) shows that the DSMC results accurately capture the slip-flow limit even for large Stokes numbers. For high Stokes number flows there are deviations from the linear velocity profile, and the velocity amplitude distribution loses its symmetry beyond $\beta=1.0$ for $\mathrm{Kn}=0.1$ flow. High Stokes number cases ($\beta \geqslant 5$) result in bounded Stokes layers, where the flow is confined to a near-wall region. Significant velocity slip can be observed with increased Stokes number beyond the quasisteady flow limit, while the slip velocity for quasisteady flows is independent of the Stokes number, as can be deduced by comparing the $\beta \leqslant 1.0$ cases with the $\beta \geqslant 5$ cases in Fig. 2(b).

Figure 3 shows the dynamic response characteristics for high Stokes number slip flow ($\mathrm{Kn}=0.1$ and $\beta=5.0$). Snapshots of velocity distribution at different times are shown in Fig. 3(a). With the exception of velocity slip, dynamics is similar to that of no-slip continuum flows. The velocity distribution predicted by the extended slip model and the DSMC simulations are in good agreement, despite a slight phase difference between the DSMC and the model. In the context of this work, the phase angle is defined as *the fraction of the time period by which the signal felt at any streamwise position lags or leads the reference velocity signal imposed on the oscillating wall*. The general representation of the velocity signal at any arbitrary location y is given by

$$u(y,t)=u_0 \sin(\omega t+\psi), \tag{26}$$

where ψ is the phase angle. Expanding and rearranging Eq. (26), we obtain

$$\begin{aligned} u(y,t) &= u_0[\sin(\omega t)\cos\psi+\cos(\omega t)\sin\psi] \\ &= A(y)\sin(\omega t)+B(y)\cos(\omega t), \end{aligned} \tag{27}$$

where

$$A(y)=u_0 \sin\psi, \quad B(y)=u_0 \cos\psi. \tag{28}$$

The phase angle can then be determined from Eq. (28) as

$$\psi(y)=\tan^{-1}\left[\frac{B(y)}{A(y)}\right]. \tag{29}$$

Following Hadjiconstantinou,[10] we use a χ-square fit to determine the coefficients A and B, given by Eq. (28), using the DSMC results. For a detailed exposition of χ-square fits and the corresponding expressions to evaluate A and B, the reader is referred to Hadjiconstantinou[10] and Press *et al.*[20]

A theoretical expression for the phase angle of the extended slip model can be derived using Eq. (29). The resultant expression is given by

$$\psi=\tan^{-1}\left[\frac{Q_2Q_3-Q_1Q_4}{Q_1Q_3+Q_2Q_4}\right], \tag{30}$$

where

$$Q_1 = q_1 + \frac{p}{\sqrt{2}}(q_3 - q_4), \quad Q_2 = q_2 + \frac{p}{\sqrt{2}}(q_3 + q_4),$$

$$p = \beta \alpha_m \, \mathrm{Kn},$$

$$Q_3 = \hat{q}_1 - p^2 \hat{q}_2 + \sqrt{2} p (\hat{q}_3 - \hat{q}_4),$$

$$Q_4 = \hat{q}_2 + p^2 \hat{q}_1 + \sqrt{2} p (\hat{q}_3 + \hat{q}_4),$$

$$q_1 = \sinh\left(\frac{1}{\sqrt{2}}\frac{\beta y}{L}\right)\cos\left(\frac{1}{\sqrt{2}}\frac{\beta y}{L}\right),$$

$$\hat{q}_1 = \sinh\left(\frac{\beta}{\sqrt{2}}\right)\cos\left(\frac{\beta}{\sqrt{2}}\right),$$

$$q_2 = \sinh\left(\frac{1}{\sqrt{2}}\frac{\beta y}{L}\right)\cos\left(\frac{1}{\sqrt{2}}\frac{\beta y}{L}\right),$$

$$\hat{q}_2 = \cosh\left(\frac{\beta}{\sqrt{2}}\right)\sin\left(\frac{\beta}{\sqrt{2}}\right),$$

$$q_3 = \cosh\left(\frac{1}{\sqrt{2}}\frac{\beta y}{L}\right)\cos\left(\frac{1}{\sqrt{2}}\frac{\beta y}{L}\right),$$

$$\hat{q}_3 = \cosh\left(\frac{\beta}{\sqrt{2}}\right)\cos\left(\frac{\beta}{\sqrt{2}}\right),$$

$$q_4 = \sinh\left(\frac{1}{\sqrt{2}}\frac{\beta y}{L}\right)\sin\left(\frac{1}{\sqrt{2}}\frac{\beta y}{L}\right),$$

$$\hat{q}_4 = \sinh\left(\frac{\beta}{\sqrt{2}}\right)\sin\left(\frac{\beta}{\sqrt{2}}\right).$$

Figure 3(b) shows the velocity time history at various streamwise locations (y/L) in the flow domain. The velocity signal at different y/L locations exhibit reduced amplitudes and different phase angles. Note that the peak values of the velocity signal in Fig. 3(b) correspond to the velocity amplitudes in Fig. 2. In Fig. 3(c), the phase angle predicted by the extended slip model and DSMC show similar trends. However, the initial deviation at $y/L \geqslant 0.9$, due to the Knudsen layer effects, offsets the DSMC results from the model solution. The phase angle variation is essentially linear in most of the domain except within the Knudsen layers near the walls. The wave propagation speed c' (phase speed) can be computed from the phase angle variation using the relation $c' = \omega/(\Delta\psi/\Delta y)$. Consequently, the phase speed, computed using the above definition, is constant in the region of linearly varying phase angle.

The extended slip model predicts a wave propagation speed of $c' = 1.770$, which is in good agreement with the corresponding DSMC prediction of $c' = 1.790$. the classical Stokes' second problem without the stationary wall also predicts a very similar wave propagation speed $c' = 1.777$. The phase speed is not constant near the walls due to the presence of Knudsen layers. In addition, the phase speed decays near the stationary wall, due to the interference between the incident and reflected signals. The normalized velocity amplitude, plotted in log scale in Fig. 3(d), shows exponential decay in the amplitude with small alterations when $y/L \leqslant 0.1$, due to the presence of the stationary wall. It can be seen that the slip model result and DSMC solution are consistent.

1. Effects of statistical scatter

Figure 3(d) aids in better visualization of statistical scatter in the DSMC results, which is insignificant for this case even near the stationary wall ($y/L \leqslant 0.1$). Note that the normalized amplitude does not drop below 1% of the maximum signal for this case. In our simulations we have observed the onset of statistical fluctuations, when the normalized signal amplitude drops below 1% of the maximum signal. Some of our DSMC results presented later in this section exhibit statistical fluctuations. In order to explore the statistical fluctuations induced by finite sampling in the presence of thermal fluctuations, we follow the recent work of Hadjiconstantinou *et al.*[21] According to the *equilibrium statistical mechanics*, the ratio of excitation velocity u_0 to the thermal fluctuation u' for an ideal gas is given by[21,22]

$$\frac{u_0}{\sqrt{\langle (u')^2 \rangle}} = \mathrm{Ma}\sqrt{\gamma N_0}, \tag{31}$$

where Ma is the Mach number, γ is the ratio of specific heats, and N_0 is the average number of particles per single cell. The velocity fluctuation is defined as $u' = u - \langle u \rangle$, where u is the instantaneous velocity and $\langle u \rangle$ is the average velocity. Since the unsteady DSMC algorithm uses ensemble average over M repeating runs, the "noise-to-signal" ratio E_u can be expressed as

$$E_u = \frac{\sqrt{\langle (u')^2 \rangle}}{u_0} = \frac{1}{\mathrm{Ma}\sqrt{\gamma M N_0}}. \tag{32}$$

Based on the above definition, and our typical simulation parameters ($u_0 = 100$ m/s, $M = 5000$, $N_0 = 100$, and $\gamma = 5/3$), we obtain $E_u = 3.4 \times 10^{-3}$. Considering that the above expression is obtained for a medium in equilibrium, the noise level in our study is expected to be higher due to the presence of strong nonequilibrium effects in high Stokes number rarefied flows.

B. Transition flow regime

Figure 4 shows the effect of Stokes number on the velocity amplitude in the transition flow regime. At fixed Kn, the slip velocity increases with increasing β. For Kn = 1.0, it can be seen that beyond $\beta = 0.25$ the quasisteady approximation breaks down. We observe a "bounded Stokes layer" type of behavior for $\beta \geqslant 5$ in both figures. Comparing the Kn = 1.0 and Kn = 2.5 cases, we find that the slip velocity increases with increasing Kn at constant β. For a fixed Kn, the Stokes layer thickness decreases with increasing β. This is an expected result.

The effect of Kn on the velocity amplitude for moderate Stokes number conditions is shown in Fig. 5. It can be seen that the slip velocity magnitude on the oscillating wall increases with increasing Kn for a fixed Stokes number. For

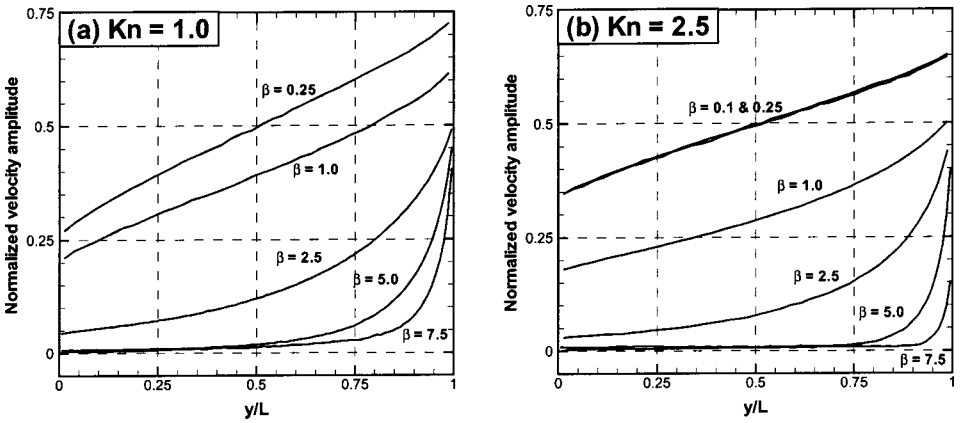

FIG. 4. Effect of β in transition flow regime.

$\beta=1.0$, quasisteady flow behavior is observed for Kn$=0.1$ [velocity amplitude distribution is linear and passes through $(y/L,u/u_0)=(0.5,0.5)$]. Hence, the quasisteady flow approximation also depends on the Kn, as can be deduced by comparison of Figs. 4 and 5. The most interesting observation in Fig. 5 is the emergence of a "*bounded rarefaction layer*" with increasing Kn. By this name we emphasize that this behavior is due to the rarefaction effects alone, and not due to the influence of the Stokes number, which is kept constant. Transition to this bounded rarefaction layer occurs even at moderate Stokes number flows [see Fig. 5(a)] by increasing the Kn. However, these effects are more pronounced when the Stokes number increases, as can be deduced by comparing Figs. 5(a) and 5(b).

Figures 6, 7, and 8 show the dynamic response of the system for moderate and high Stokes number flows in the transition flow regime (Kn$=1.0$, $\beta=2.5$; Kn$=1.0$, $\beta=5.0$, and Kn$=5.0$, $\beta=2.5$). Here, we will not present detailed discussions of the dynamic system response for the individual cases, since the behavior is qualitatively similar to that of Fig. 3. Comparing Figs. 6(a) and 7(a), we observe that a more pronounced Stokes layer forms by increasing the Stokes number. Alternatively comparing Figs. 6(a) and 8(a), we observe a more pronounced bounded rarefaction layer, when the Kn is increased. In all three cases, reduced velocity amplitudes and different phase angles are observed at different streamwise locations. Note that, while the phase angle reaches 210° at $y/L=0$ in Fig. 6(c), the same value is reached at $y/L\simeq0.75$ in Fig. 7(c), and at $y/L\simeq0.8$ in Fig. 8(c). This indicates that the phase speed, as defined earlier in this paper, increases with increasing β and Kn. It is also worthwhile to compare the level of statistical scatter between these three results. Statistical scatter in Fig. 6(d) is insignificant, since the normalized velocity amplitude does not drop below 1% of the signal. However, with increasing β and Kn, the normalized velocity amplitude drops below 1% outside the "bounded layers," and the statistical scatter becomes important, as can be observed in Figs. 7(d) and 8(d). These findings are consistent with our predictions based on Eq. (32).

C. Free-molecular flow regime

Validation of the DSMC results in the free-molecular flow regime is presented in Fig. 9. We compare the normalized velocity amplitudes obtained from the DSMC with the solution of the linearized collisionless Boltzmann equation at different Stokes numbers. The free-molecular solution plotted in this figure is obtained from Eq. (22). Overall, a very good agreement between the DSMC results and the free-molecular solution is obtained. Here, we must note that we utilized DSMC with finite Kn, instead of the test particle Monte Carlo Method (TPMC) commonly utilized for collisionless flows.[6] The DSMC results in Fig. 9(a), show statis-

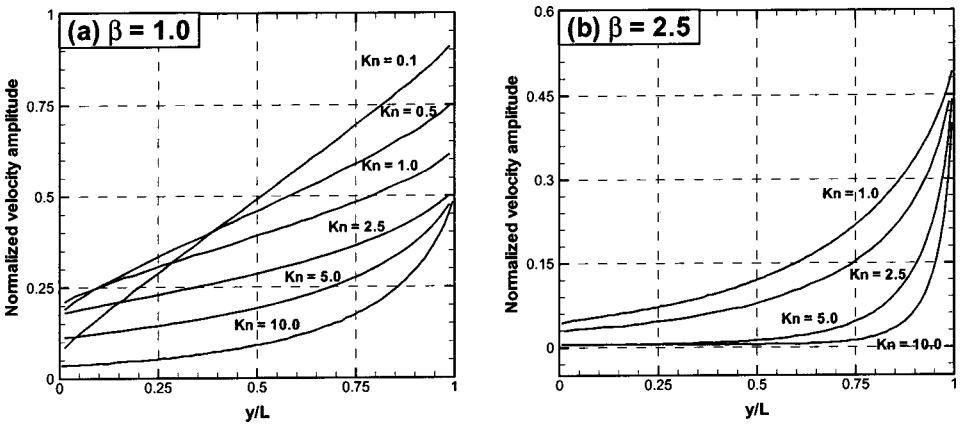

FIG. 5. Effect of Kn for moderate β condition.

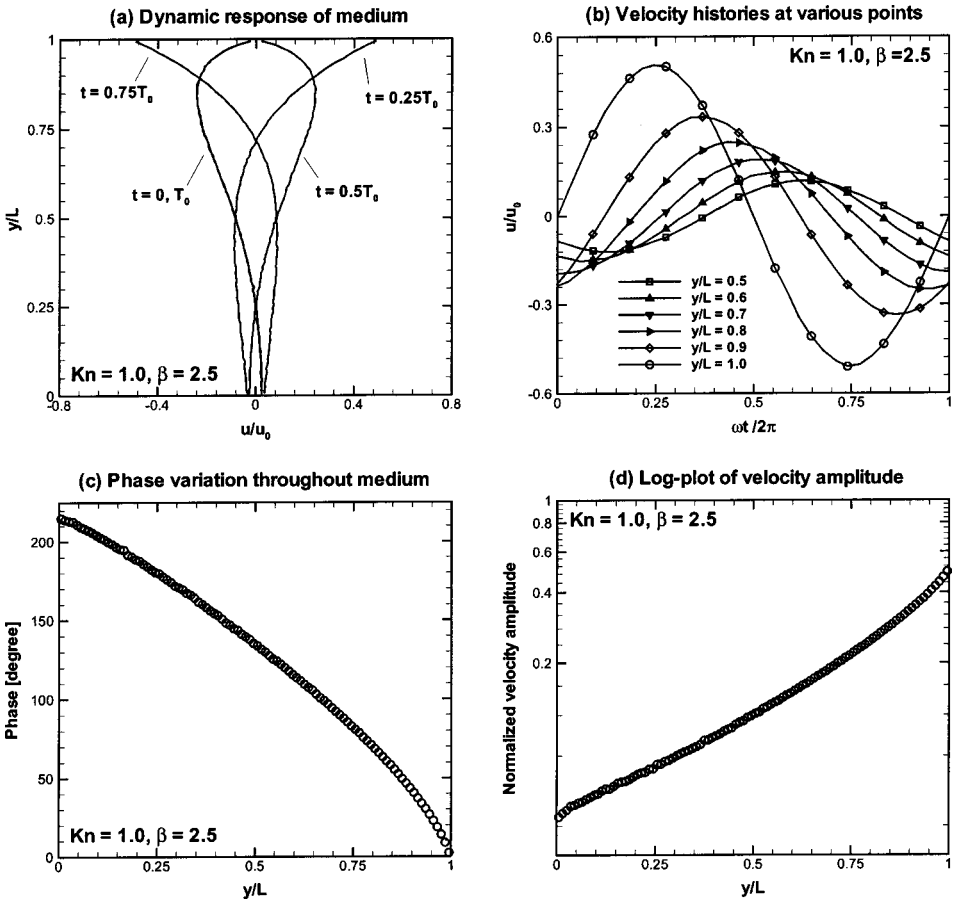

FIG. 6. Dynamic details for Kn=1.0 and $\beta=2.5$ flow.

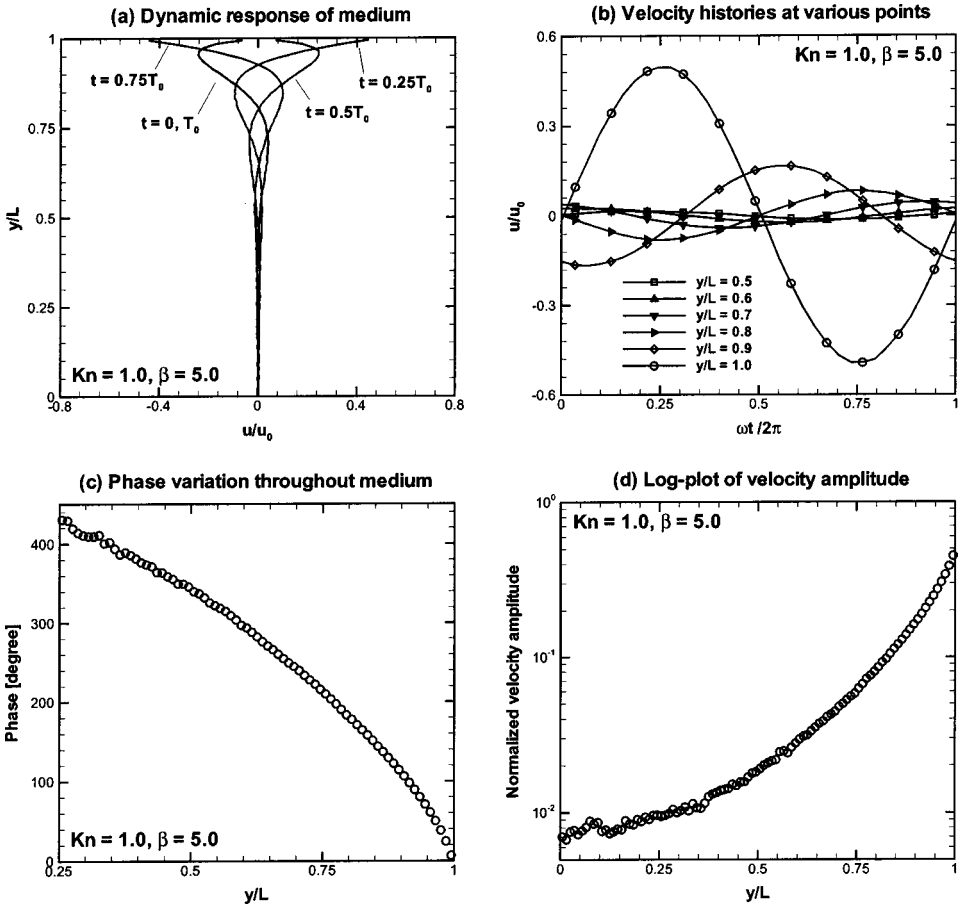

FIG. 7. Dynamic details for Kn=1.0 and $\beta=5.0$ flow.

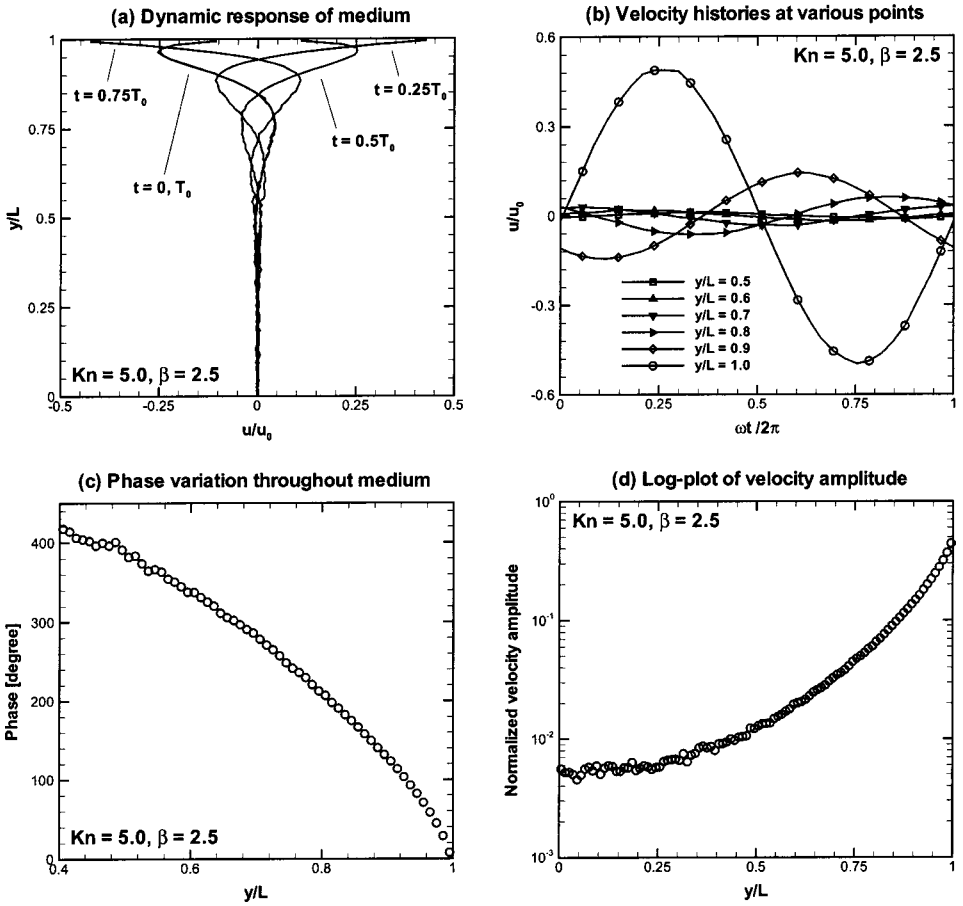

FIG. 8. Dynamic details for Kn=5.0 and $\beta=2.5$ flow.

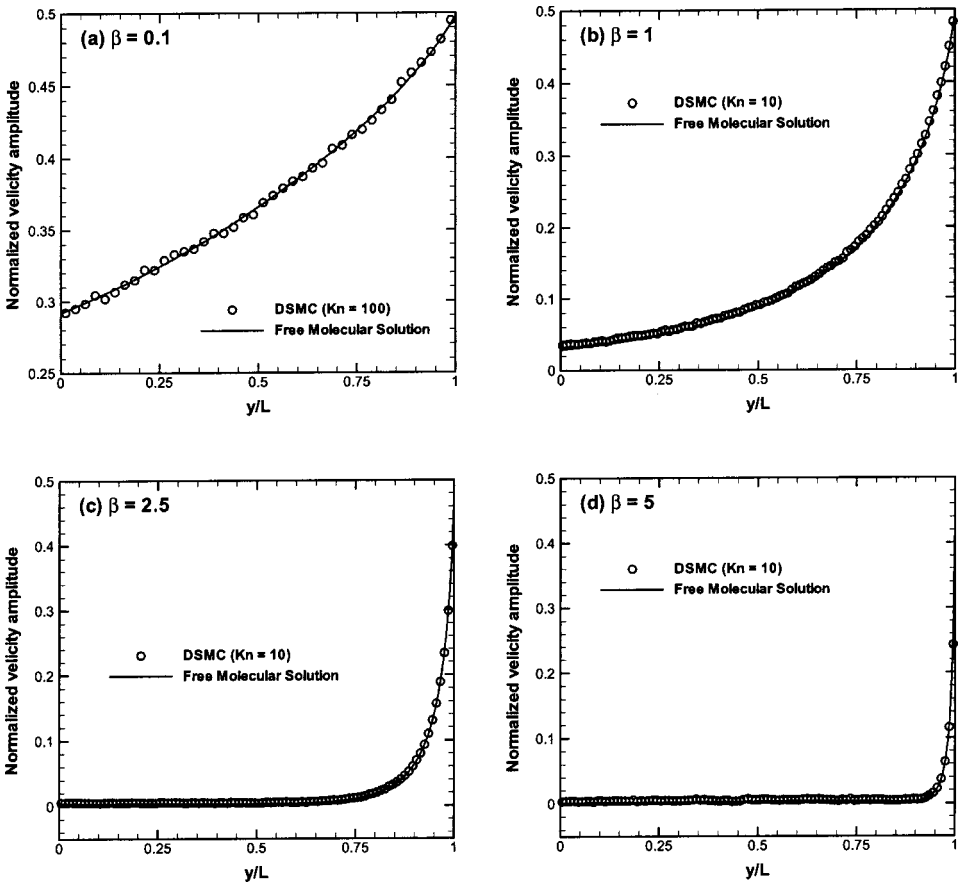

FIG. 9. Velocity amplitudes for free-molecular flow regime.

tical scatter associated with a high Knudsen number simulation. However, agreement between the theory and simulations are remarkable in Figs. 9(b)–9(d).

In Figs. 10 and 11, we compare the dynamic response of the medium obtained from the DSMC results and the collisionless Boltzmann equation solutions for Kn=10, $\beta=1.0$, and Kn=10, $\beta=2.5$ cases. Predictions of the velocity profiles, phase angles, and the slip velocities are presented in the figures. As observed in Fig. 11(a), both methods capture the bounded rarefaction layer equally well. Due to the onset of statistical scatter outside this layer, we plotted the DSMC phase angle only for $y/L \geqslant 0.65$, in Fig. 11(c). Nevertheless, the DSMC and Boltzmann solutions match remarkably well with in the bounded layer, confirming the accuracy of our DSMC results.

D. Penetration depth

It is important to note that the bounded Stokes and rarefaction layers observed in the results create a new length scale in the problem. This new length scale is related to the thickness of the Stokes/rarefaction layers, and becomes particularly important for high values of Kn or β. The Stokes layer thickness ($\delta \approx \sqrt{\nu/\omega}$), also referred to as the ''penetration depth'' is defined as the distance from the moving wall where the velocity amplitude decays to 1% of its excitation value ($u/u_0=0.01$). Most flow is confined within this layer, and the moving wall no longer interacts with the stationary wall. For these cases, the characteristic length scale of the problem should be based on the penetration depth δ, rather than the separation distance between the two plates. This would require redefinition of the nondimensional parameters Kn and β, based on the penetration depth ($\mathrm{Kn}'=\lambda/\delta, \beta'=\sqrt{\omega\delta^2/\nu}$). However, there are no functional relations for variation of δ as a function of Kn and β. Hence, *a priori* estimation of the penetration depth is not possible. For the sake of consistency, Kn and β are defined using the plate separation distance throughout this work. Hence, no switch is made in the characteristic length scale. However, change in the characteristic length scale has physical implications. For example, the actual Knudsen number for these cases can be found by $\mathrm{Kn}'=\mathrm{Kn}\,L/\delta$. Figure 12 shows variation of the normalized penetration depth (δ/L) with Kn and β. For the cases not shown in this figure, the signal does not attenuate enough to observe a bounded layer. The penetration depth decreases with increasing β, as expected. The penetration depth asymptotes to different values in the free-molecular limit for different Stokes numbers. For fixed β, the penetration depth decreases by increasing the Kn, reflecting the ''bounded rarefaction layer'' concept presented above. It can be seen from Fig. 12 that $\delta/L \propto 1/\mathrm{Kn}$ for a given β. This figure also clarifies the need for a redefinition of the characteristic length scale for high β and Kn flows.

E. Shear stress

Shear stress for oscillatory Couette flows exhibits two distinct behaviors in the continuum and free-molecular flow

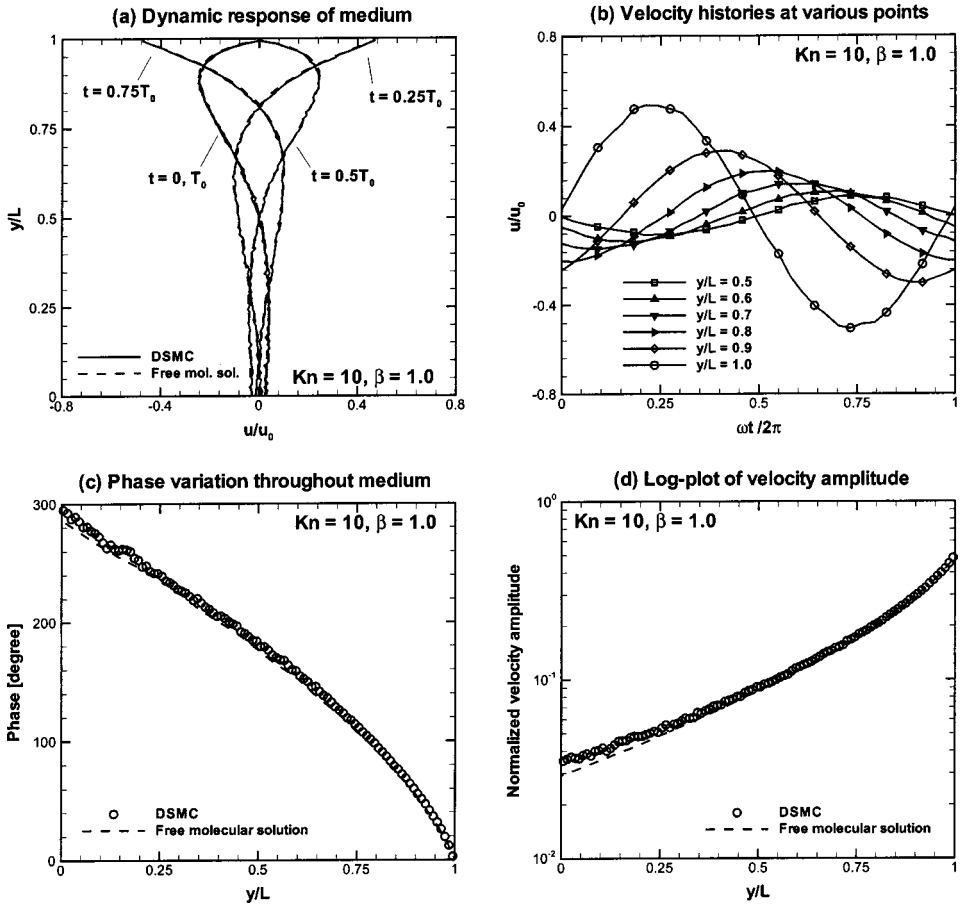

FIG. 10. Dynamic details for Kn=10 and $\beta=1.0$ flow.

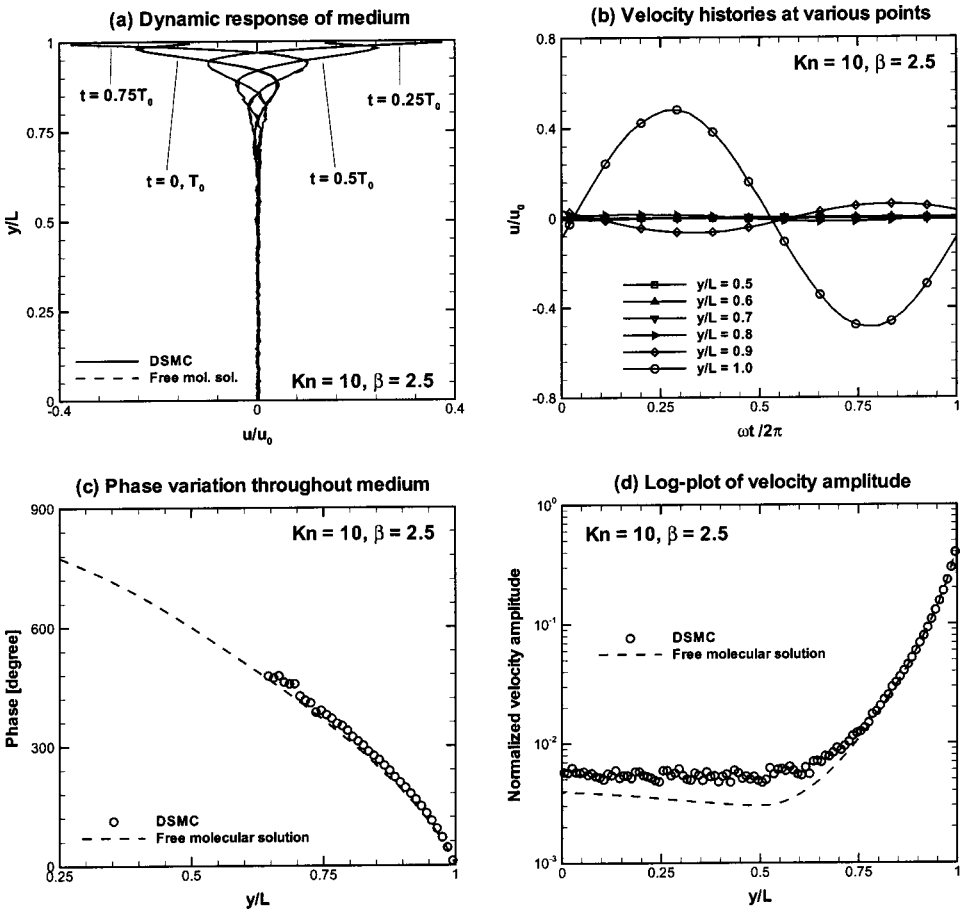

FIG. 11. Dynamic details for Kn=10 and $\beta=2.5$ flow.

regimes. Using the classical constitutive laws utilized in the Navier–Stokes equations, the continuum shear stress is given by

$$\tau_{\text{cont}}=\mu_{\text{HS}}\frac{u_0}{L}, \tag{33}$$

where μ_{HS} is the hard-sphere viscosity ($\mu_{\text{HS}}=5/16d_{\text{HS}}^2\sqrt{mk_BT_e/\pi}$). The hydrodynamic approximation of shear stress is proportional to the velocity gradient (angular deformation rate for 1D flow). This representation is also valid in the slip-flow regime with the appropriate velocity slip corrections. The free-molecular shear stress can be obtained from Eq. (25) as

$$\tau_{\text{FM}}=\frac{1}{2}\rho_0 u_0\sqrt{\frac{2k_BT_e}{\pi m}}. \tag{34}$$

Note that this is *identical* to the free-molecular shear stress, obtained for steady plane Couette flows.[23] In Fig. 13, we present the effect of Kn and β on the wall shear stress using the DSMC results. We plot the shear stress normalized with the free-molecular and continuum shear stress values, to show that the DSMC results uniformly approach the correct asymptotic limits. We also compare the DSMC results with our empirical model for quasisteady oscillatory flows given by Eq. (7). Good agreements between the empirical model and the DSMC results are observed for quasisteady flows ($\beta\leqslant 0.25$). Beyond the quasisteady flow regime there is a significant increase in the shear stress magnitude, especially for low Kn values. This is expected, since the shear stress is proportional to the velocity gradient, which increases with β, especially due to the formation of bounded Stokes layers. In the free-molecular flow limit, shear stress reaches the same asymptotic limit of the steady plane Couette flow regardless of the Stokes number, as shown in Eq. (25). In Fig. 13, we observed a similar behavior in the DSMC results. Interest-

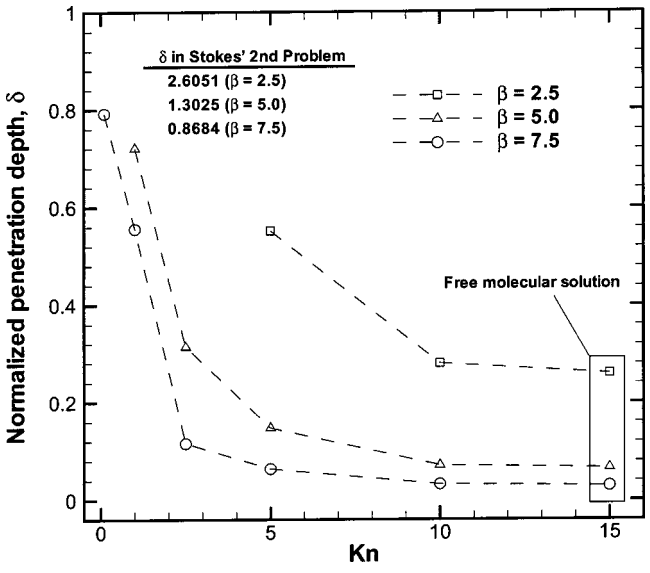

FIG. 12. Effects of Kn and β on penetration depth.

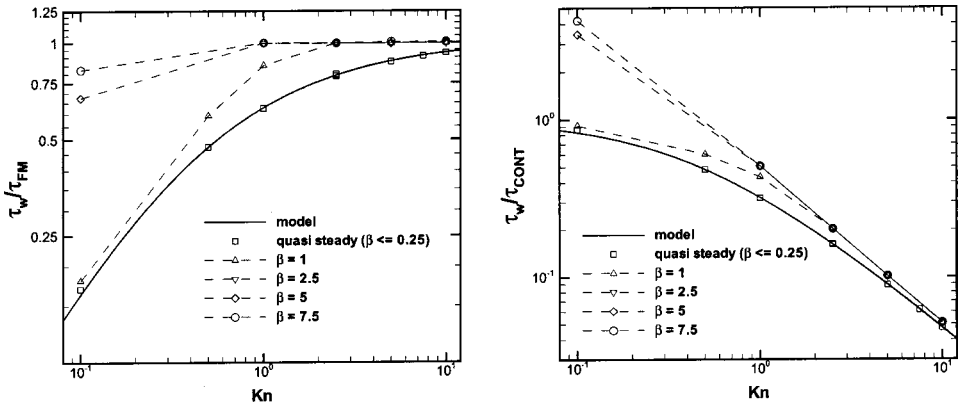

FIG. 13. Effects of Kn and β on wall shear stress.

ingly, the DSMC data reached the asymptotic shear stress value in the transition flow regime for large Stokes number cases. This behavior is a manifestation of our definition of Kn which is constant regardless of β. If we consider changing the characteristic length scale from the distance between the two plates (L) to the penetration length (δ), we would observe that the effective Knudsen number for such cases are indeed in the free-molecular flow regime. For example, for the Kn$=2.5$, $\beta=7.5$ case, the penetration depth $\delta=0.15L$ (see Fig. 12). Hence, the effective Knudsen number for this case is about Kn$\simeq 17$.

VI. CONCLUDING REMARKS

Time-periodic Couette flows are studied in the entire Knudsen regime and a wide range of Stokes numbers using the unsteady DSMC method. To our knowledge this is the first time that unsteady DSMC have been utilized for this basic flow. The DSMC results are validated using analytical solution of the linearized collisionless Boltzmann equation in the free-molecular flow regime, and a recently developed empirical model in the slip-flow regime. We paid particular attention to the statistical scatter in the simulations, which became important when the velocity signal is reduced below 1% of the maximum signal. This was sufficient to accurately resolve the velocity signal in most of the flow domain, including the bounded Stokes layers.

Simulations show that the quasisteady flow conditions, which result in linear velocity distribution with equal velocity slip on the oscillating and stationary surfaces, diminish beyond a certain Stokes number. Although this limit also depends on the Kn, we generally suggest $\beta\leqslant 0.25$ as the limit for quasisteady flows. The empirical model presented in Ref. 14 is also valid in this regime for Kn$\leqslant 12$, and it can be easily substituted in place of the DSMC simulations. For moderate Stokes number flows, we observe oscillatory Couette flow between the two walls. At these intermediate β values, two surfaces interact with each other, and the aforementioned empirical model is valid only in the slip-flow regime.

For high Stokes number flows, we observed formation of bounded Stokes layers, where the stationary wall does not interact with the flow anymore. In the slip-flow regime, this results in the classical Stokes' second problem with velocity slip. Once again, the empirical model in Ref. 14 is valid in this regime, where the wave speed is constant outside the Knudsen layer, and the velocity amplitude decays exponentially as a function of the distance from the oscillating surface. However, there are small deviations from this behavior within the Knudsen layer. Such deviations are captured by the DSMC, but they cannot be modeled using continuum-based approaches. In the transition and free-molecular flow regimes we observed that the signal decay is not exactly exponential and the wave speed is not constant anymore. These are interesting deviations, which are also validated using the analytical solution of linearized collisionless Boltzmann equation in the free-molecular flow limit. In all simulations, the results have consistently shown that the slip velocity and wave propagation speed increase with increased Kn and β.

An interesting behavior is observed when the Kn is increased while the Stokes number is fixed. For such cases, the slip velocity increases, and a bounded layer with a finite penetration depth is formed after a certain value of Kn. We named this the bounded rarefaction layer. Penetration depth for this layer is a function of both Kn and β, and it becomes a new length scale in the problem. For such cases, it is necessary to redefine the Knudsen number based on the penetration depth, rather than the separation distance between the two plates. However, without *a priori* knowledge of the penetration depth it is not possible to predetermine the Kn in the simulations. In order to remain consistent, we kept the characteristic length scale of the problem as the plate separation distance. However, the reader can use Fig. 12 to estimate the actual Knudsen number based on the penetration depth. Due to this switch in the length scales, we observed that shear stress on the oscillating wall reaches the asymptotic free molecular limit at earlier Kn values. Solution of the linearized collisionless Boltzmann equation in the free-molecular flow limit indicates that the shear stress and the slip velocity amplitude for oscillatory Couette flows are *identical* to that of the steady plane Couette flows. This interesting finding is also confirmed by our DSMC results.

ACKNOWLEDGMENTS

J.H.P. acknowledges support by the Postdoctoral Fellowship Program of Korea Science & Engineering Foundation (KOSEF). We are also grateful to Professor Felix Sharipov for many useful discussions and suggestions regarding the

current study. Computational resources provided by Professor Seung Wook Beak at Korea Advanced Institute of Science and Technology (KAIST) is greatly appreciated.

[1]K. S. Breuer, ''Lubrication in MEMS,'' in *The MEMS Handbook*, edited by M. Gad-el-Hak (CRC Press, Washington, DC, 2002), pp. 1–27.
[2]Y. H. Cho, A. P. Pisano, and R. T. Howe, ''Viscous damping model for laterally oscillating microstructures,'' J. Microelectromech. Syst. **3**, 81 (1994).
[3]C. T.-C. Nguyen and R. T. Howe, ''An integrated CMOS micromechanical resonator high-Q oscillator,'' IEEE J. Solid-State Circuits **34**, 440 (1999).
[4]T. Veijola and M. Turowski, ''Compact damping models for laterally moving microstructures with gas-rarefaction effects,'' J. Microelectromech. Syst. **10**, 263 (2001).
[5]M. Gad-el Hak, ''The fluid mechanics of microdevices—the Freeman Scholar Lecture,'' J. Fluids Eng. **121**, 5 (1999).
[6]G. A. Bird, *Molecular Gas Dynamics and Direct Simulation of Gas Flows* (Oxford University Press, Oxford, 1994).
[7]W. Wagner, ''A convergence proof for Bird's direct simulation Monte Carlo technique,'' J. Stat. Phys. **66**, 1011 (1992).
[8]S. Stefanov, P. Gospondinov, and G. Cercignani, ''Monte Carlo simulation and Navier–Stokes finite difference calculation of unsteady-state rarefied gas flow,'' Phys. Fluids **10**, 289 (1998).
[9]N. G. Hadjiconstantinou and A. L. Garcia, ''Molecular simulations of sound wave propagation in simple gases,'' Phys. Fluids **13**, 1040 (2001).
[10]N. G. Hadjiconstantinou, ''Sound wave propagation in transition-regime micro- and nanochannels,'' Phys. Fluids **14**, 802 (2002).
[11]F. Sharipov, W. Marques, and G. M. Kremer, ''Free molecular sound propagation,'' J. Acoust. Soc. Am. **112**, 395 (2002).
[12]J. H. Park and S. W. Baek, ''Investigation of influence of thermal accommodation on oscillating micro-flow,'' Int. J. Heat Mass Transfer (in press).
[13]J. H. Park, S. W. Baek, S. J. Kang, and M. J. Yu, ''Analysis of thermal slip in oscillating rarefied flow by using DSMC,'' Numer. Heat Transfer, Part A **42**, 647 (2002).
[14]P. Bahukudumbi, J. H. Park, and A. Beskok, ''A unified engineering model for shear driven gas micro flows,'' Microscale Thermophys. Eng. **7**, 291 (2003).
[15]C. Loudon and A. Tordesillas, ''The use of the dimensionless Wormersley number to characterize the unsteady nature of internal flow.'' J. Theor. Biol. **191**, 63 (1998).
[16]A. G. Straatman, R. E. Khayat, E. Haj-Qasem, and D. A. Steinman, ''On the hydrodynamic stability of pulsatile flow in a plane channel,'' Phys. Fluids **14**, 1938 (2002).
[17]R. L. Panton, *Incompressible Flow*, 2nd ed. (Wiley, New York, 1996).
[18]Y. Sone, ''Kinetic theory analysis of linearized Rayleigh problem,'' J. Phys. Soc. Jpn. **19**, 1463 (1964).
[19]Y. Sone, ''Effect of sudden change of wall temperature in rarefied gas,'' J. Phys. Soc. Jpn. **20**, 222 (1965).
[20]W. H. Press, S. A. Teukolsky, W. T. Vetterling, and B. P. Flannery, *Numerical Recipes in* FORTRAN, 2nd ed. (Cambridge University Press, Cambridge, 1992).
[21]N. G. Hadjiconstantinou, A. Garcia, M. Bazant, and G. He, ''Statistical error in particle simulations of hydrodynamic phenomena,'' J. Comput. Phys. **187**, 274 (2003).
[22]L. D. Landau and E. M. Lifshitz, *Statistical Physics* (Pergamon, New York, 1980).
[23]M. Kogan, *Rarefied Gas Dynamics* (Plenum, New York, 1969).